Supplementary information

Cubic SnGe Nanoalloys: Beyond Thermodynamic Composition Limit

Karthik Ramasamy,*[a] Paul G. Kotula,[b] Norman Modine,[b] Michael T. Brumbach,[b] Jeffrey M. Pietryga,[c] Sergei A. Ivanov

Materials

All reagents were used as received, and the solvents were dried over molecular sieves and purged with high purity argon for 30 minutes before use. Germanium (II) diiodide (GeI_2), was purchased from Gelest Inc. Tin (II) bis(trimethylsilyl)amide ($Sn(HMDS)_2$, ≥ 99.0%), bis(N,N'-diisopropylacetamidinato) tin(II), $Sn(DIPAA)_2$ and oleylamine (OLA, ≥80-90.0%) were obtained from Sigma Aldrich Chemical Co and Acros Organics. 2M *n*-butyllithium solution in cyclohexane, anhydrous hexane and anhydrous methanol were purchased from Sigma Aldrich Chemical Co.

Characterization

Routine transmission electron microscopy (TEM) imaging was performed using a FEI-Tecnai, 300 kV transmission electron microscope equipped with a CCD camera for scanning transmission electron microscopy (STEM), a high-angle annular dark field (HAADF) detector, and energy-dispersive Scanning transmission electron microscopy X-ray (EDX) spectroscopy. The High Temperature TEM measurements were conducted on FEI-Tecnai instrument and the d(111) values were collected from multiple nanocrystals on a same sample. The measurements were repeated twice for each sample to confirm the observation. Scanning transmission electron microscopy (STEM) high-angle annular dark field imaging and EDX elemental mapping were performed using and FEI Company Titan G2 80-200 TEM/STEM operated at 200kV and equipped with the X-FEG (an ultra-stable high-brightness Schottky FEG source), Super-X EDX detector system (4 windowless silicon drift detectors with a combined solid angle of 0.7 sr) and a spherical aberration corrector (CEOS DCOR) on the probe-forming optics. TEM image non-linear processing - Fourier filtering - was carried out using Gatan Digital Micrograph version 3.4. Scanning electron microscope (SEM) imaging was carried out using a Focused Ion Beam Scanning Electron Microscope (FIB-SEM, Carl Zeiss) equipped with EDX.

Powder X-ray diffraction (XRD) patterns and small angle X-ray scattering (SAXS) were recorded on a Rigaku Smart Lab II instrument equipped with Cu Kα radiation source operated at 40 kV and 44 mA. Samples for powder XRD measurements were covered with Paratone-N crystallographic oil to prevent excessive oxidation and deposited on the horizontal glass slide. Samples for SAXS were dissolved in

hexane and the solution was loaded into 0.7mm boron glass capillaries for measurements. PDXL v2.0 and NANO-Solver v3.5 software packages from Rigaku were used to process the powder XRD and SAXS data, respectively. SAXS data were modeled as Gamma distribution of spherical particles with normalized dispersion, σ, referred to as *'size distribution'* throughout the rest of the text: $\sigma[\%]=(\langle\delta R^2\rangle/\langle R\rangle^2)^{1/2}100\%$.

XPS measurements was performed using a Kratos Axis Ultra DLD instrument with base pressures less than $5 \cdot 10^{-9}$ Torr. Samples for XPS were mounted onto a sample holder in a glove box and briefly (< 5 sec.) exposed to air in transfer from the glove box to the instrument. XPS was performed with a monochromatic Al Kα (1486.7 eV) source operated at 150 W with an elliptical spot size of 300 x 700 microns. Survey spectra were recorded with an 80 eV pass energy, 600-700 meV step sizes, and 100 ms dwell times. High resolution spectra were recorded with a 20 eV pass energy, 50 meV step sizes, and 100 ms dwell times. Charge neutralization was used for all samples to reduce differential charging effects. Data processing was performed with CasaXPS Version 2.3.15. Spectra were adjusted to align the C 1s peak to 284.6 eV. Sn 3d peaks and Ge 3d peaks have been normalized and smoothed to allow for direct comparison between samples. A linear background was applied to the Sn 3d 5/2 peak and the Ge 3d peak. Absorption measurements were carried out using a Cary 6000i dual-beam UV-Vis-NIR spectrometer. PL spectra were taken using a homebuilt setup: excitation from an 808 nm laser was mechanically chopped, and emission was analyzed using a grating monochromator and a LN_2-chilled InSb detector using lock-in amplification. Proton decoupled ^{119}Sn NMR spectra were acquired using Anasazi EFT 90MHz instrument with the reference ^{119}Sn frequency (0 ppm) set at 33.66574 MHz. Samples were dissolved in pure oleylamine. The acquisition time of 5000 scans, the relaxation delay, and the pulse width were set to 0.14ms, 0.20ms, and 10μs, respectively.

Theoretical assessment

In order to gain insights into the possible mechanism for the suppression of Sn-Ge phase separation in formed nanoparticles, we have performed preliminary molecular dynamics (MD) simulations based on the Kohn-Sham Density Functional Theory (DFT) [W. Kohn and L. J. Sham, Phys. Rev. **140**, A1133 (1965).]. These calculations used the Socorro electronic structure software [See http://dft.sandia.gov/socorro], the Local Density Approximation (LDA) [D. M. Ceperley and B. J. Alder, Phys. Rev. Lett. **45**, 566 (1980); J. P. Perdew and Y. Wang, Phys. Rev. B **45**, 13244 (1992).], and a plane-wave basis set with a 30 (120) Rydberg cutoffs for wave functions (densities and potentials). In order to promote the formation of a crystalline Ge region, we constructed the initial structures for our MD simulations by placing Sn and Ge atoms on the sites of a 256- atom supercell consisting of a 4x4x2

repetition of the diamond-structure 8-atom cubic unit cell. Subsequently, two vacancies were introduced into Sn rich regions in these supercells in order to serve as nucleation sites for melting. In order to obtain adequate sampling of the Brillouin zone, our calculations used two k-points along the x2 direction of the supercell. The temperature was controlled during MD using the Hoover implementation of the Nose thermostat [See *Understanding Molecular Simulation* by D. Frenkel and B. Smit (Academic Press, 2002, San Diego CA) for details of the algorithm.]. The lattice constant of the supercell was adjusted until melting of Sn rich regions was observed during MD simulations at 510 K but not at 500 K.

Synthesis of Sn_xGe_{1-x} Nanocrystals via injection method

In a typical reaction, a 3-neck round bottom flask containing 5 mL of oleylamine was degassed under vacuum and back filled with N_2 for three times. The flask was heated to a target growth temperature (between 210°C and 280°C) at which 60 μL of 2M *n*-BuLi cyclohexane solution were injected and followed by 1 mL oleyamine solution of GeI_2 (0.2 mmol) and a varied amount of $Sn(HMDS)_2$ or $Sn(DIPAA)_2$ were swiftly injected. the reaction mixture was held for a period of up to 1 hour before the reaction was quenched by the removal of the reaction flask from the heating mantle.

The NCs were collected via precipitation by addition of methanol, followed by centrifugation and redispersal in hexane.

Sulfur overcoating on Sn_xGe_{1-x} Nanocrystals

In a 3-neck round bottom flask containing 6 mL of Sn_xGe_{1-x} nanoparticle parent solution was degassed under vacuum and back filled with N_2 for three times at 100 °C. 2 mL of 10 mM S/OLA solution was introduced into the Sn_xGe_{1-x} nanoparticle solution gradually (0.5 mL/h) using syringe pump at 180 °C and particles were cleaned using hexane and methanol after sulfur overcoating.

Table 1. Tin content ***x(Sn)*** in Sn_xGe_{1-x} alloy nanocrystals determined from XRD, SEM-EDX and ICP.

Lattice Parameter (Å)	***x(Sn)*** **XRD[(1)]**	***x(Sn)*** **EDX**	***x(Sn)*** **ICP**
5.720	0.10	0.10	0.10
5.818	0.24	0.25	0.23
6.029	0.50	0.50	0.52
6.249	0.75	0.74	0.75
6.385	0.85	0.87	-
6.443	0.95	-	-

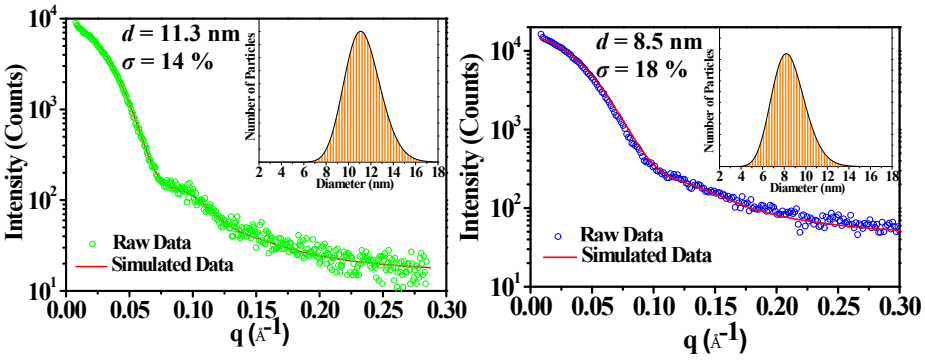

Fig S1. Small angle X-ray scattering patterns of Sn_xGe_{1-x} (x = 0.50 (a) and 0.75(b)) NCs in hexane (Inset: Particle size distribution obtained from SAXS measurements)

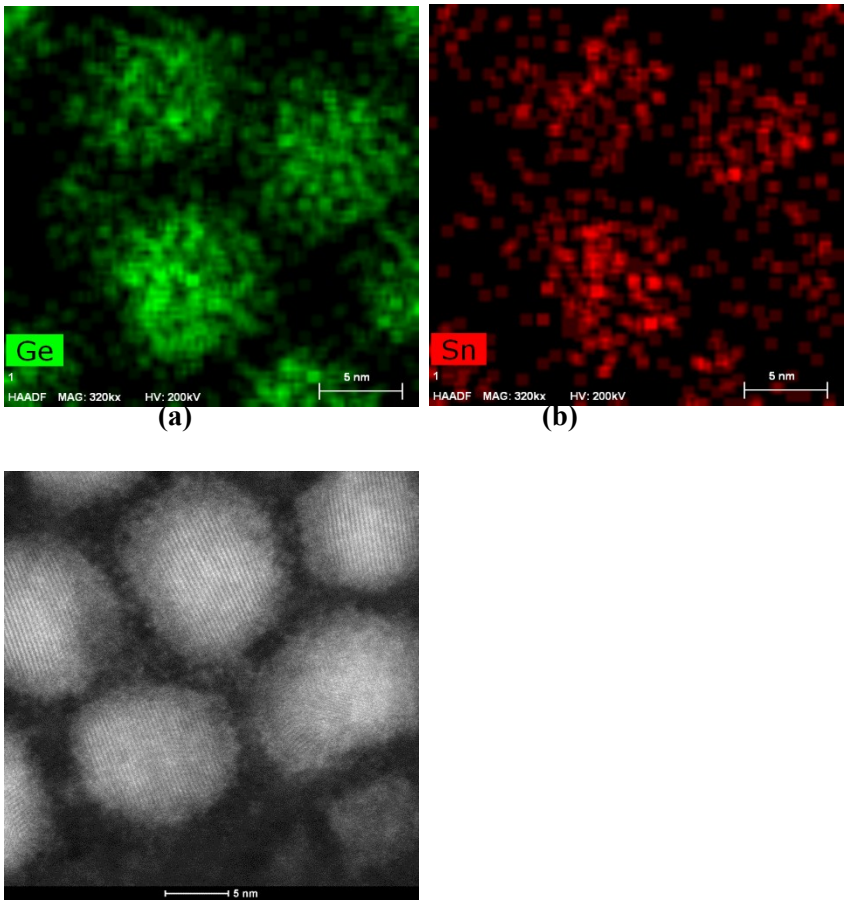

Fig S2. High magnification EDX elemental images with 5nm scale bar for Sn_xGe_{1-x} (x = 0.27) for (a) Ge and (b) Sn distributions. (c) High resolution High Angular Annular Dark Field (HAADF) image of Sn_xGe_{1-x} (x = 0.27) nanoalloys showing co-localization of tin and germanium.

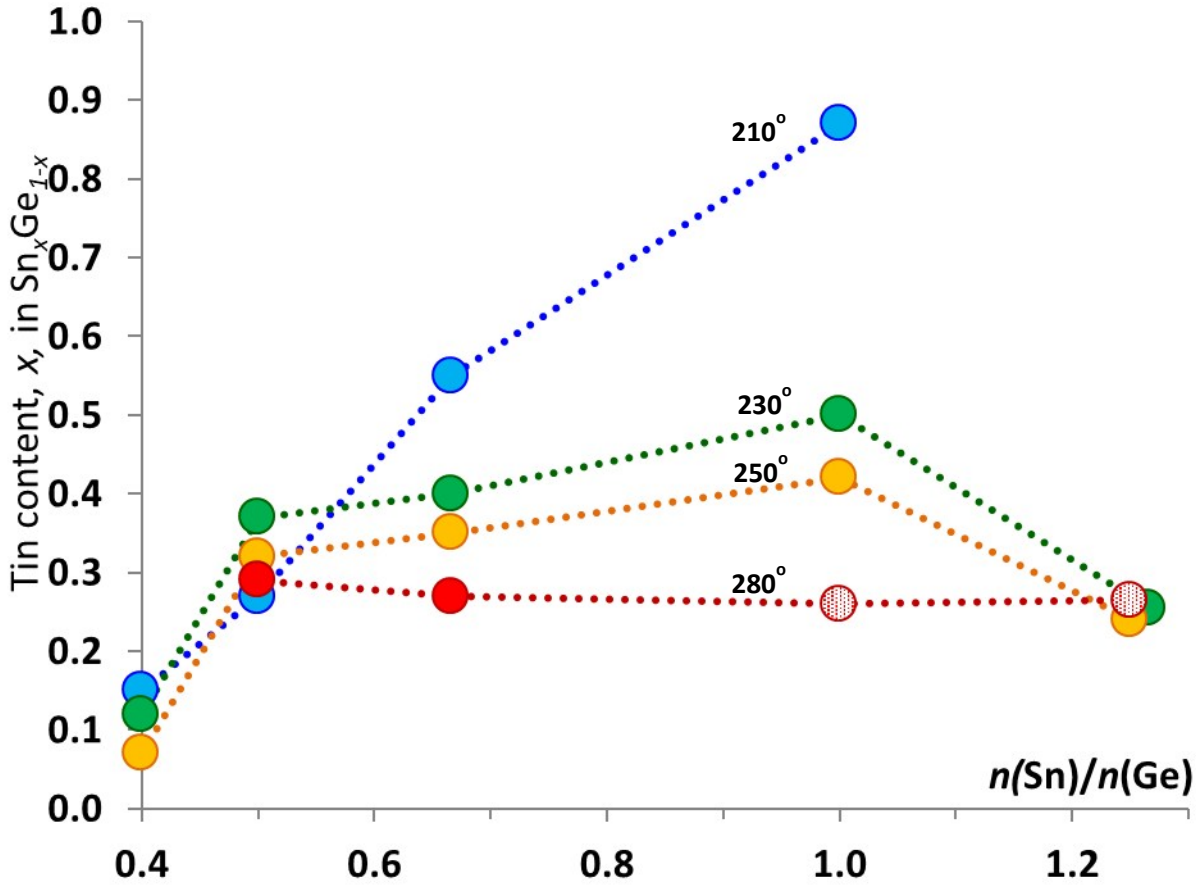

Fig S3. Variation of tin content in Sn_xGe_{1-x} nanoparticles after 10 min of growth time with varying Ge-to-Sn precursor ratio. Partially shaded circles at 280°C indicate the contamination with beta-Sn phase. The diagram identifies the 1:1 ratio as the optimal value for the widest composition control of the final product via growth temperature.

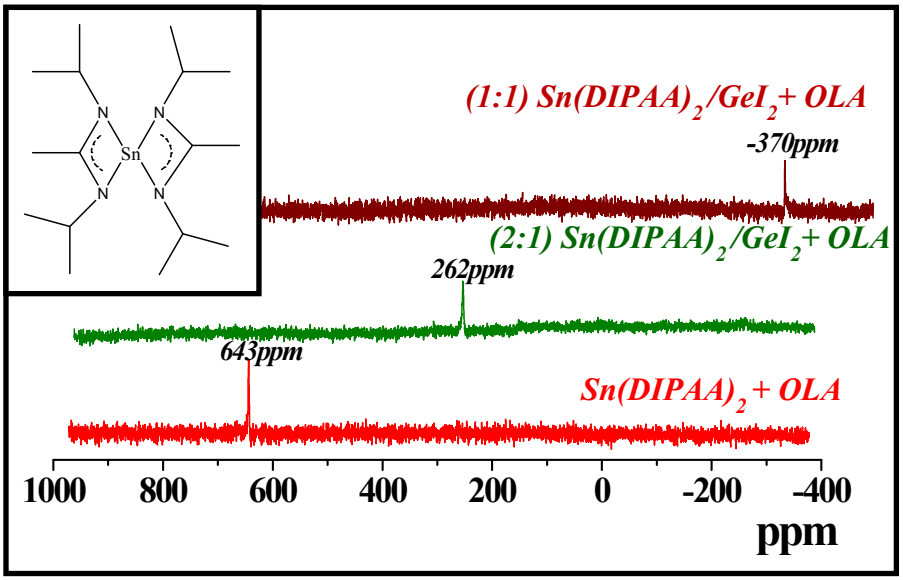

Fig S4. Room temperature $^{119}Sn\{^{1}H\}$ NMR spectra of the mixture of $Sn(DIPAA)_2$ and GeI_2 in oleylamine.

The ^{119}Sn NMR was used to assess the possibility of a mix-metal complex formation upon mixing of Sn and Ge precursors as recently it was proposed that combining tin(II) and germanium(II) complexes of HMDS in dodecylamine (DDA) leads to the formation of binary cubane-like imides $Sn_xGe_{4-x}(\mu_3\text{-}L)_4$ ($L=C_{12}H_{25}N$).[30] Although our assessment of the reported system by means of ^{119}Sn NMR did not reveal the formation of mix-metal cubanes at Sn:Ge ratios up to 1:8, larger amounts of $Ge(HMDS)_2$ indeed led to the formation of $Sn_3Ge(\mu_3\text{-}L)_4$ ($L=C_{12}H_{25}N$). We believe that a similar process occurs upon mixing of $Sn(HMDS)_2$ (or $Sn(DIPAA)_2$) with GeI_2 in OLA. Although ^{119}Sn resonances in toluene solutions of $Sn(HMDS)_2$ and $Sn(DIPAA)_2$ possess drastically different chemical shifts (+678ppm and –252ppm for $Sn(HMDS)_2$ and $Sn(DIPAA)_2$, respectively), the dissolution of both precursors in neat OLA produces the singlet in ^{119}Sn NMR spectrum at +644ppm (Figure S3), which can be attributed to the formation of homometallic $Sn_4(\mu_3\text{-}L)_4$ ($L=C_{18}H_{35}N$), the assignment that is also supported by the observation of septets in ^{1}H NMR spectra in accordance with previous observations.[30] Introduction of GeI_2 to the tin precursor solution in OLA leads to the disappearance of the cubane signal and the appearance of a new singlet upfield at +260ppm or +300ppm (for the solution with $Sn(DIPAA)_2$ or $Sn(HMDS)_2$, respectively). Increase in the amount of GeI_2 added to tin beyond Ge/Sn=2:1 ratio eventually leads to the disappearance of the singlet and increase in resonance at -370ppm, which is close to the signal of pure SnI_2 in OLA (-364ppm). The latter appeared to be stable even after heating to 200 °C.

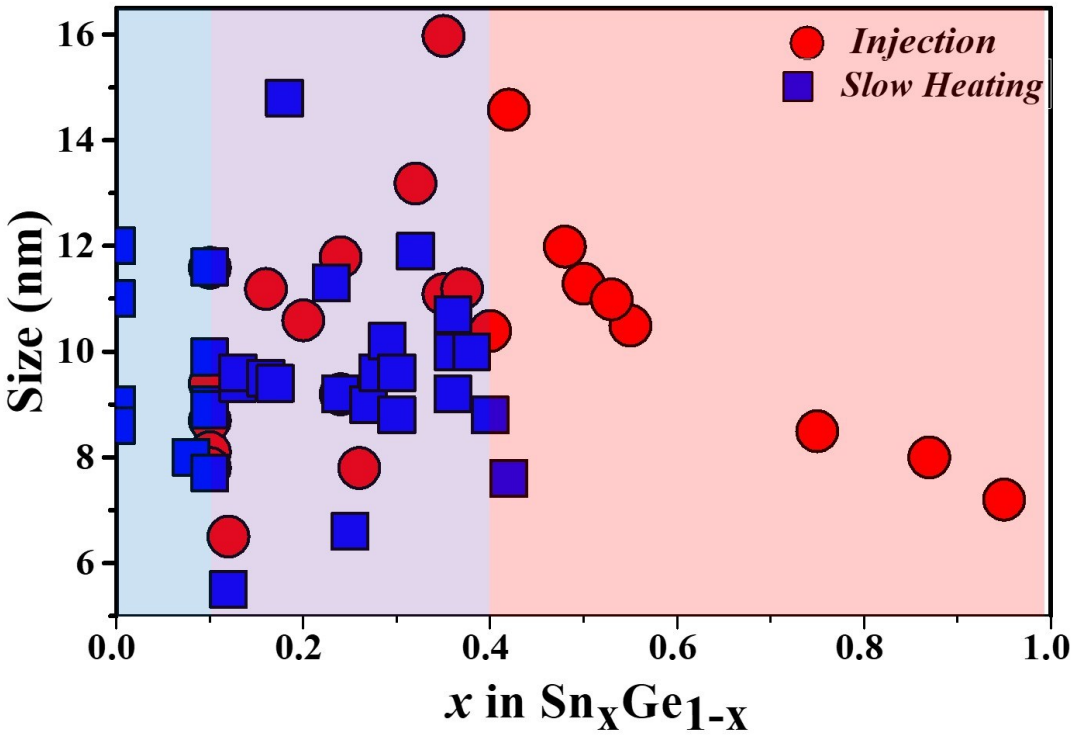

Fig S5. Distribution of size+composition combinations achieved for SnxGe1-x nanoparticles synthesized via the slow heating (blue squares) and hot injection (red circles) methodologies (precursors ratios, temperatures and reaction times varied). As can be seen, the achievable variation for either method is quite broad, and either can be used for nanoparticles containing 10-40% tin (purple shading), but slow heating is best for even lower contents (blue shading), and the hot-injection method is uniquely capable of producing higher tin contents (red shading).

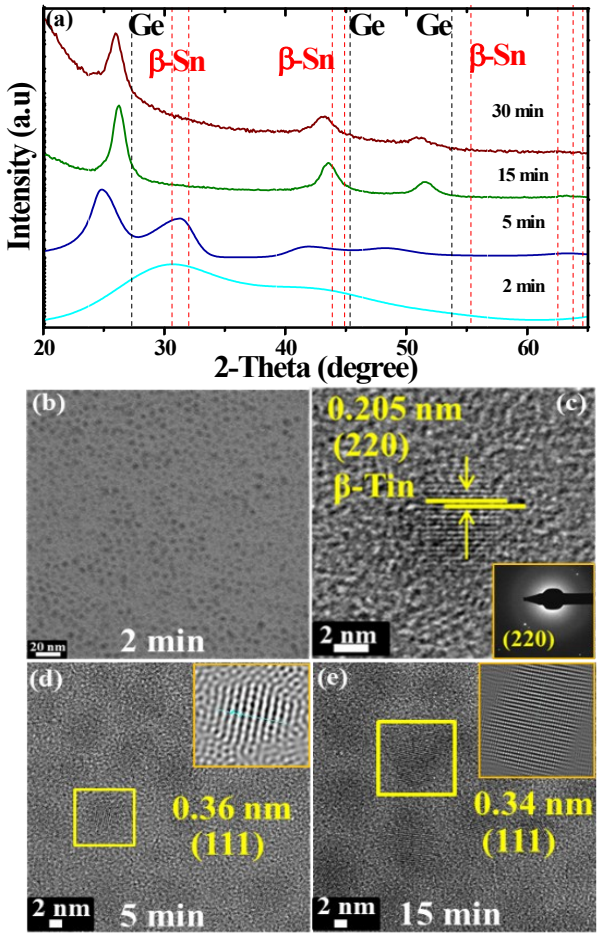

Fig S6. (a) XRD of NCs isolated at different time intervals. Red and black dotted lines correspond to diffraction positions of pure β-Sn and Ge, respectively. (b) TEM image of NCs isolated after 2 min. (c) HRTEM image. Inset: Selected area electron diffraction pattern attributed to β-Sn NCs. (d) and (e) TEM images of NCs isolated after 5 and 15 mins, respectively. Insets: Inverse FFT images of respective TEM images

Table S2. Representative experimental conditions for the synthesis of Sn_xGe_{1-x} nanocrystals via the injection method discussed in the main text and in the supplementary information section.

Ge:Sn in reaction mixture	Ge:BuLi	Lattice Constant (Å)	*x* in Sn_xGe_{1-x}	Temp (°C)	Time (min)	Size, nm	Size Distribution, %
1	No BuLi used	5.720	0.10	230	60	8.7	22
1	3.3	5.928	0.38	230	60	11.8	14
1	3.3	6.029	0.50	230	30	11.3	14
1	3.3	6.249	0.75	230	20	8.5	18
1	3.3	6.385	0.87	210	30	8.0	20
1	3.3	6.443	0.95	210	20	7.2	23
1	3.3	6.070	0.55	210	60	10.5	21
1	3.3	6.011	0.48	250	20	12.0	24
1	3.3	5.960	0.42	250	30	14.6	21
1	3.3	5.902	0.35	250	60	16.0	18
1	3.3	-	0.32 + β tin	280	20	-	-
1	3.3	-	0.26 + β tin	280	30	-	-
1	3.3	-	0.18 + β tin	280	60	-	-
0.5	3.3	-	β tin	210	30	-	-
0.8	3.3	-	β tin	210	30	-	-
1.5	3.3	6.069	0.55	210	30	7	24
2.0	3.3	5.844	0.27	210	30	8.4	22
2.5	3.3	5.752	0.15	210	30	6.4	20
0.5	3.3	-	β tin	230	30	18.0	19
0.8	3.3	5.836	0.26	230	30	7.8	24
1.5	3.3	5.942	0.40	230	30	10.4	21
2.0	3.3	5.918	0.37	230	30	11.2	19
2.5	3.3	5.733	0.12	230	30	8.2	21
0.5	3.3	-	β tin	250	30	24.0	21
0.8	3.3	5.818	0.24	250	30	9.2	22
1.5	3.3	5.902	0.35	250	30	11.1	24
2.0	3.3	5.878	0.32	250	30	13.2	21
2.5		5.696	0.07	250	30	10.1	19
0.5	3.3	-	β tin	280	30	-	-
0.8	3.3	-	0.26 + β tin	280	30	-	-
1.5	3.3	5.846	0.27	280	30	14	22
2.0	3.3	5.856	0.29	280	30	16	20
2.5	3.3	-	No rxn	280	30		
3.0	No Reaction						

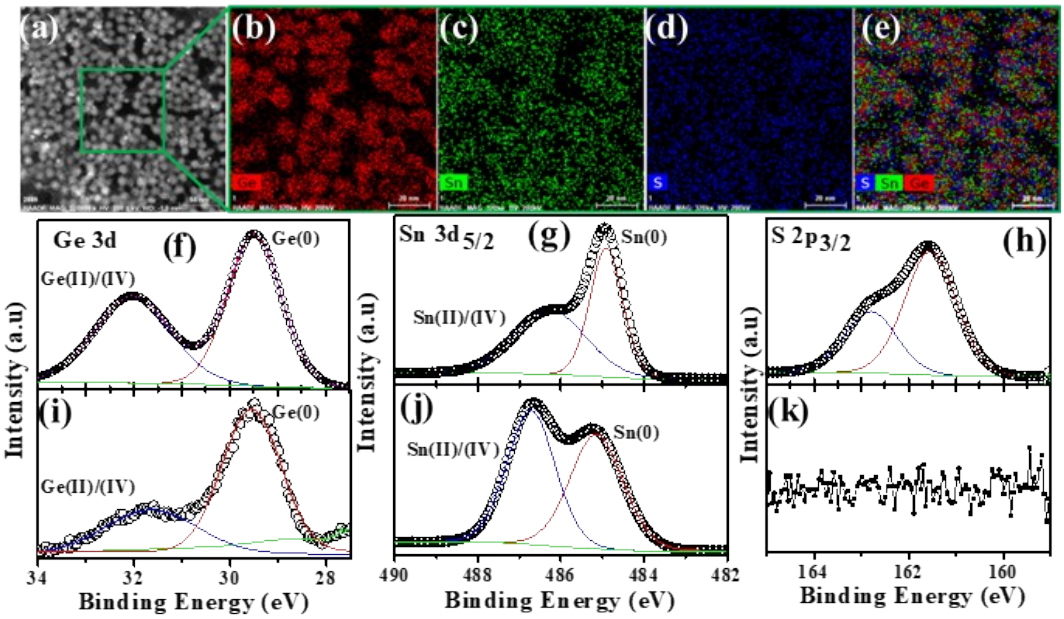

Fig S7. (a) HAADF image of sulfur-treated Sn_xGe_{1-x} NCs with x = 0.36. (b)-(d) STEM-EDX mapping images of Sn, Ge and S from the boxed area in (a). Combined image of (b)-(d) panels indicating co-localization of three elements. High-resolution XPS spectra (normalized linear intensity) of Ge 3d, Sn $3d_{5/2}$ and S $2p_{3/2}$ electrons, respectively, for (f)-(h) the sulfur-treated and (i)-(k) pristine Sn_xGe_{1-x} alloy NCs. Oxidation states of all three elements are indicated next to the corresponding peak component of the experimentally measured spectral envelope (black line)

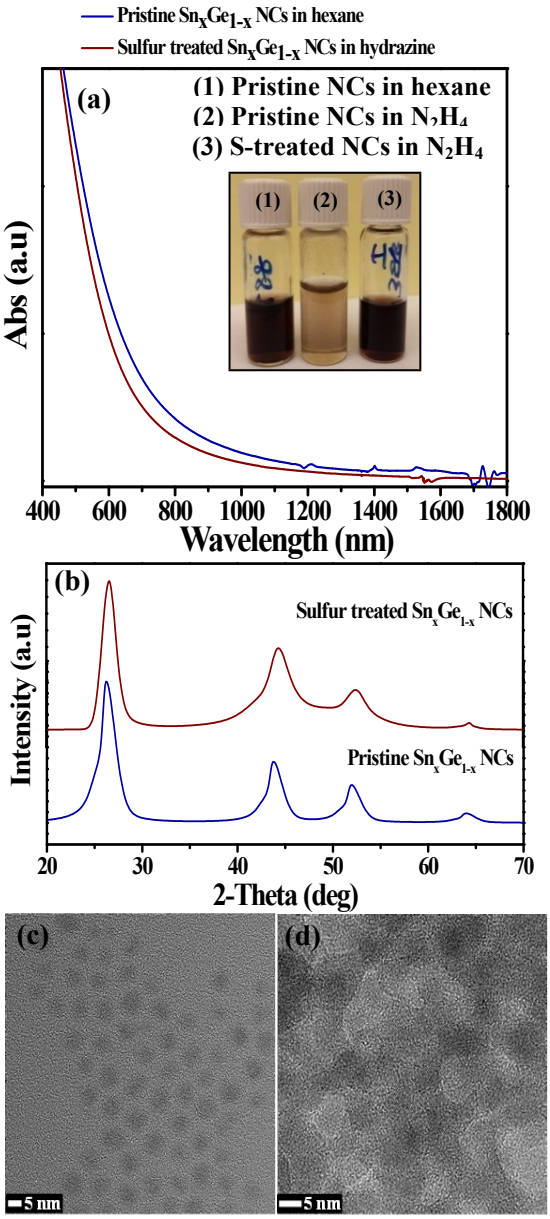

Fig S8. (a) Absorption spectra of pristine and sulfur treated NCs. Inset shows vials containing pristine Sn_xGe_{1-x} NCs in hexane and in hydrazine, and sulfur treated NCs in hydrazine. (b) X-ray diffraction patterns of pristine and sulfur treated Sn_xGe_{1-x} NCs with x = 0.36. (c) & (d) transmission electron microscope images of pristine and sulfur treated Sn_xGe_{1-x} NCs with x = 0.36.

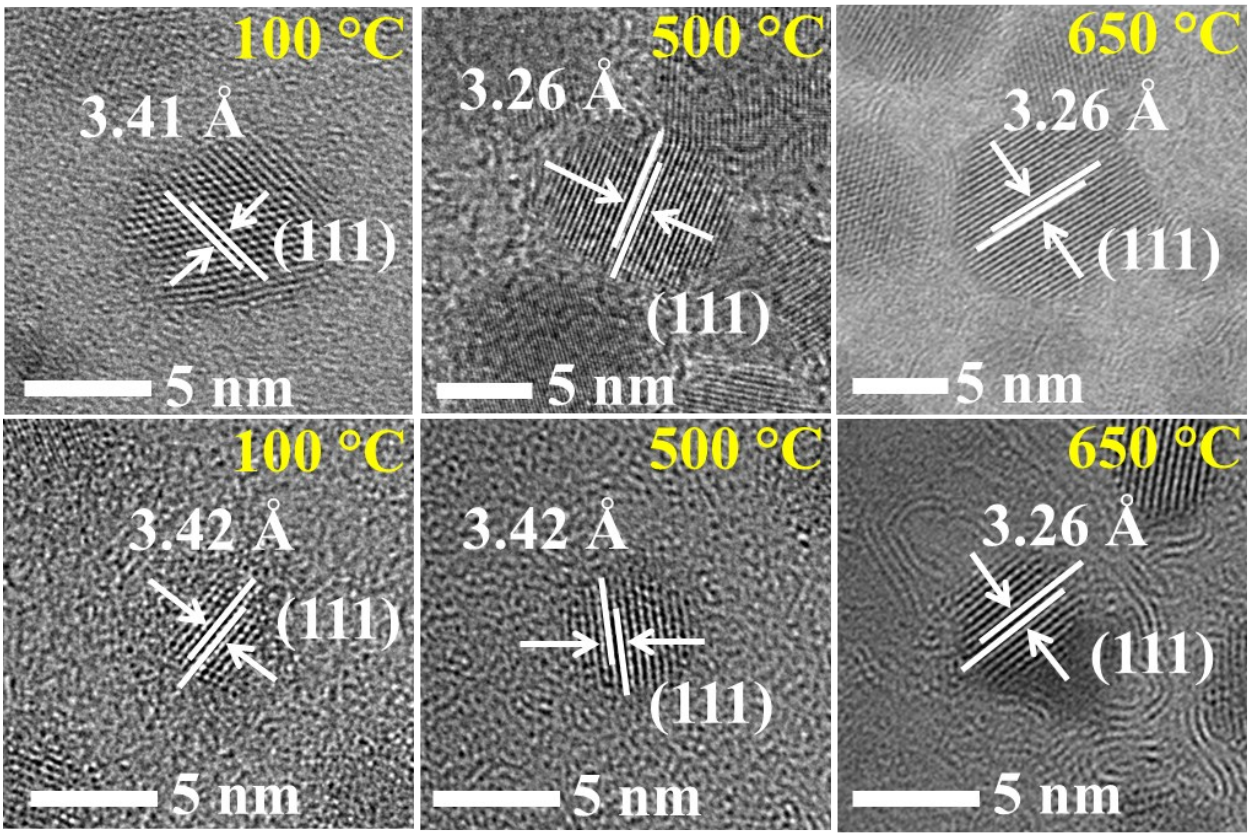

Fig S9. TEM images of (a-c) untreated and (d-f) sulfur coated Sn_xGe_{1-x} NCs at different temperatures. Samples were held for 10 min at each temperature. There is an apparent stability of d(111) value characteristic of alloy at 500°C in S-coated particles as opposed to not treated particles, where d(111) value is equal to that of pure germanium.